



UNIVERSIDAD DISTRITAL
FRANCISCO JOSÉ DE CALDAS

Visión Electrónica

<https://doi.org/10.14483/issn.2248-4728>







VISIÓN ELECTRÓNICA

A RESEARCH VISION

Integrated computational analysis of digital photoelasticity and thermoelastic stress analysis

Análisis computacional integrado de fotoelasticidad digital y análisis termoelástico de esfuerzos

Yeins Yefferson Aristizabal-López ¹, Juan Carlos Briñez de León ², Alejandro Restrepo-Martínez ³,
Hermes Alexander Fandiño-Toro ⁴

INFORMACIÓN DEL ARTÍCULO

Historia del artículo:

Enviado: 24/11/2021

Recibido: 09/12/2021

Aceptado: 12/02/2022

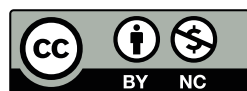
Keywords:

Fringe density

Load stepping

Stress field

Temperature field



Palabras clave:

Densidad de franjas

Load stepping

Campos de esfuerzos

Campos de temperatura

ABSTRACT

Stress measurement is useful to identify the operating conditions that can produce the failure of a structure. Among the strategies for stress measurement, the integration between digital photoelasticity and thermoelastic stress analysis has been extensively explored, because it is useful to determine the individual stresses, and because of its full-field capabilities. However, due to the experimental complexity of both techniques, their integration is often limited to semi-static cases, where the calibration of the thermal parameters is usually done independently of the photoelasticity experiment. This paper describes a novel computational integration of digital photoelasticity and thermoelastic stress analysis. The main contribution of the paper is to show that, under controlled conditions, the application of variable load can be used to determine the stress and temperature fields of a birefringent model. The results achieved of this paper could be useful in industrial environments, where the complexity of the experiments limits the range of applications that require stress field analysis.

RESUMEN

La medición de los esfuerzos mecánicos es importante en múltiples aplicaciones de ingeniería porque permite identificar las condiciones de operación que hacen que las piezas fallen. Dentro de las estrategias para medir esfuerzos mecánicos la integración de la fotoelasticidad digital y el análisis termoelástico de esfuerzos ha sido ampliamente explorada, porque permite obtener información de esfuerzos individuales y no solo de su suma o diferencia; y porque permite análisis no invasivos y de campo completo. Sin embargo, dada la complejidad experimental de ambas técnicas, su integración suele limitarse a casos semi-estáticos donde la calibración de los parámetros térmicos se suele hacer independientemente al montaje de fotoelasticidad. Este trabajo explora una integración computacional novedosa de la fotoelasticidad digital y el análisis termográfico de esfuerzos mediante la aplicación de carga variable a un modelo birrefringente. Los resultados obtenidos indican que, bajo condiciones controladas, es posible obtener simultáneamente los campos de esfuerzos y de temperaturas del modelo inspeccionado. Estos resultados podrían ser de útiles entornos industriales, donde la complejidad de los experimentos limita el rango de aplicaciones que requieren análisis de campos de esfuerzos.

¹BSc. (c) in electronic engineering, Instituto Tecnológico Metropolitano, Colombia. E-mail: yeinsaristizabal207546@correo.itm.edu.co

²BSc. in electronic engineering, Universidad de Pamplona, Colombia. MSc. in Industrial Automation and Control, Instituto Tecnológico Metropolitano, Colombia. Professor at Institución Universitaria Pascual Bravo, Colombia. E-mail: juan.brinez@pascualbravo.edu.co

³BSc. in mechanical engineering, Universidad Nacional de Colombia, Medellín, Colombia. PhD. in engineering, Universidad Nacional de Colombia, Medellín, Colombia. Professor at: Universidad Nacional de Colombia, Medellín, Colombia. E-mail: arestre5@unal.edu.co

⁴BSc. in electronic engineering, Universidad Nacional de Colombia, Manizales, Colombia. MSc. In engineering, Universidad Nacional de Colombia, Manizales, Colombia. Professor at Instituto Tecnológico Metropolitano, Colombia. E-mail: hermesfandino@itm.edu.co

Cite this article as: Y. Y. Aristizabal-López, J. C. Briñez de León, A. Restrepo-Martínez, H. A. Fandiño-Toro, "Integrated computational analysis of digital photoelasticity and thermoelastic stress analysis", *Visión Electrónica*, vol. 16, no. 1, pp. 16-28, 2022. <https://doi.org/10.14483/22484728.17313>

1. Introduction

Mechanical stresses indicate how a force is distributed within the geometry of a part or structure. Their evaluation is of importance in a wide range of engineering applications because it allows the identification of the operating conditions that cause parts to fail. However, this evaluation is not simple given the set of methods that must be implemented, integrated and synchronized in order to individualize the required information. Among the strategies reported in the literature to evaluate and separate stress information, the integration of digital photoelasticity studies and thermoelastic stress analysis has been widely explored. However, given the experimental complexity of each method, their implementation has been limited to semi-static cases where the calibration of the thermal parameters is usually estimated asynchronously and independently of the photoelasticity setup.

This paper shows a strategy to integrate photoelasticity and thermoelastic stress analysis. To show that the proposed integration is theoretically possible, computational experiments were performed where the application of variable load to a birefringent model produced sufficient information to calculate its stress and thermal fields. Both photoelasticity and thermoelastic stress analysis are useful to evaluate the mechanical performance of structures under load, with the advantage that they allow non-destructive and full-field analyses.

In photoelasticity, the stress field of a birefringent object is obtained by processing fringe patterns on its surface. The shape and intensity of these patterns is related to the difference of principal stresses at the considered spatial location. Photoelasticity has been shown to be useful in fracture mechanics problems, in stress analysis of static and moving mechanical components [1], in residual stress analysis [2], in biomedical applications, and in general in full-field stress analysis.

Thermoelastic Stress Analysis (TSA) is a technique for quantifying the temperature changes exhibited by an object under cyclic loading [3-4]. Among other applications, TSA is used in the early detection and characterization of delaminations, cracking and other types of surface defects in multiple materials, and to predict the service life of structural components [5].

Photoelasticity and TSA provide complementary information on the stress field. While photoelasticity is

defined in terms of the difference of principal stresses, TSA is formulated in terms of their sum. Due to this complementarity, different studies have proposed the integration of these two techniques as a strategy to separate principal stresses [6-8]. Stress separation is a current problem in engineering, because in several practical applications it is necessary to know the principal stresses individually and not only their sum or difference [9]. It has been documented that only at the boundaries of the inspected objects, photoelasticity produces complete solutions; and in regions far from the boundaries, stress separation techniques must be used [10].

Although stress separation can also be achieved by numerical approaches, these require prior knowledge of the stress state, or boundary conditions, of the evaluated object. Additionally, numerical approaches can be affected by errors due to finite difference approximation [11].

Separately, photoelasticity and TSA have analytical and experimental requirements that must be met to provide reliable information; requirements that can make their integration difficult. In photoelasticity, stress maps are obtained after using multiple stages of processing collections of images. In experimental problems, the acquisition of the required images can be a challenge in itself, because it requires setups where the inadequate arrangement of the required optical instruments can produce errors during the stress field calculation. On the other hand, while in TSA the image acquisition setups are comparatively simple, the temperature values produced are usually small, and require the application of cyclic loading, under adiabatic conditions, and with mechanical systems that can become very expensive.

Despite these considerations, several works have succeeded in integrating photoelasticity and TSA experimentally [6], [11], [12]. For photoelastic analysis, these works used a method called phase stepping, which produces images where the parameters describing the magnitude and orientation of the principal stresses interact and had to be decoupled: isochromatic and isoclinic parameters, respectively.

In this paper, a computational experiment is proposed where a photoelastic method to reconstruct the stress field, which is based on the application of variable load, is applied fast enough to allow the reconstruction of the stress field by means of TSA. The main contributions of the presented work are

to demonstrate that the integration is theoretically possible under the proposed conditions, and to show what difficulties would be involved in an experimental implementation. To date, the authors are not aware of photoelasticity and TSA integration strategies that consider the photoelastic method considered in this work: the fringe displacement method by load variation [13]. This is relevant since the images obtained with this technique do not exhibit the interaction between the isochromatic and isoclinic parameters, and can be obtained by hybrid techniques whose implementation requires simplified optical setups [14].

2. Theoretical framework

In the experiments presented in this paper, diametral loading is applied to a polymethylmethacrylate (PMMA) disc. The experiments are computational, and are based on theoretical concepts from photoelasticity and thermoelastic stress analysis. These theoretical concepts and how to use them to obtain digital images are presented below.

2.1. Birefringence and photoelasticity

Some materials that transmit visible light have an optical property called birefringence. When an object made of a birefringent material is subjected to load, it exhibits two refractive indices. Birefringence causes phase delays in the light rays traveling through the object. These delays provide full-field information about the mechanical response of the object to the applied load. Photoelasticity provides expressions to quantify these phase delays, and to use the information from these delays to calculate the stress field of the birefringent object under inspection.

2.1.1. Mechanical stresses in a disc under diametral compression

For some models such as rectangular discs and plates, analytical expressions are known that describe the stresses at any point of their geometry, and for different types of applied load. In this paper, the model of the disk under pointwise diametral compression is considered, since it has been extensively studied in mechanical stress analysis based on photoelasticity. Equations (1), (2) and (3) indicate how to calculate the rectangular stress components and shear stresses for this model.

$$\sigma_{xx} = \frac{-2F}{\pi h} \left(\frac{x^2(R-y)}{[(R-y)^2 + x^2]^2} + \frac{x^2(R+y)}{[(R+y)^2 + x^2]^2} - \frac{1}{2R} \right) \quad (1)$$

$$\sigma_{yy} = \frac{-2F}{\pi h} \left(\frac{(R-y)^3}{[(R-y)^2 + x^2]^2} + \frac{(R+y)^3}{[(R+y)^2 + x^2]^2} - \frac{1}{2R} \right) \quad (2)$$

$$\tau_{xy} = \frac{-2F}{\pi h} \left(\frac{x(R-y)^3}{[(R-y)^2 + x^2]^2} + \frac{x(R+y)^3}{[(R+y)^2 + x^2]^2} - \frac{1}{2R} \right) \quad (3)$$

In these expressions x and y represent the rectangular coordinates of each point on the disk geometry, F is the applied force in Newtons, and R and h are the radius and thickness of the specimen, respectively. From Equations (1), (2) and (3), the principal stresses and the direction of the principal stresses can be calculated using Equations (4), (5) and (6).

$$\sigma_1 = \frac{\sigma_{xx} + \sigma_{yy}}{2} + \sqrt{\frac{(\sigma_{xx} + \sigma_{yy})^2}{2} + \tau_{xy}^2} \quad (4)$$

$$\sigma_2 = \frac{\sigma_{xx} + \sigma_{yy}}{2} - \sqrt{\frac{(\sigma_{xx} + \sigma_{yy})^2}{2} + \tau_{xy}^2} \quad (5)$$

$$\theta = \frac{1}{2} \frac{2\tau_{xy}}{\sigma_{xx} - \sigma_{yy}} \quad (6)$$

2.1.2. Optical stress law

Given a point in the geometry of a birefringent model under load, Equation (7) allows to calculate the retardation of the light traveling through that point. This equation describes the so-called Stress-Optical Law.

$$\delta = \frac{2\pi h C}{\lambda} (\sigma_1 - \sigma_2) \quad (7)$$

This law states that the phase delay is an inverse function of the wavelength λ , and that it is directly

proportional to the principal stress difference, the thickness h of the sample under consideration and its stress-optical coefficient C .

This equation applies to the case where the wavelength is constant, so its use in computational analysis will result in the generation of grayscale images. However, it is possible to extend the analysis to produce color images, using Equation (8). There, λ_1 y λ_2 refer to the minimum and maximum wavelengths of the illumination source under consideration.

$$\delta = \frac{1}{\lambda_2 - \lambda_1} \sum_{\lambda_1}^{\lambda_2} \frac{2\pi h C}{\lambda} (\sigma_1 - \sigma_2) \quad (8)$$

2.1.3. Stress field in digital photoelasticity studies

The stress field of a birefringent model under load is obtained by processing a set of images with fringe patterns, such as those obtained with equations (7) and (8). In experimental problems, the visualization of these patterns is achieved by placing the inspected sample inside an optical instrument called a polariscope, which serves to modify the polarization state of the light traveling through the sample. Figure 1 shows a circular polariscope, which consists of two linear polarizers, two quarter-wave retarders, an illumination source and a camera. The birefringent model is in the middle of the optical elements of the polariscope.

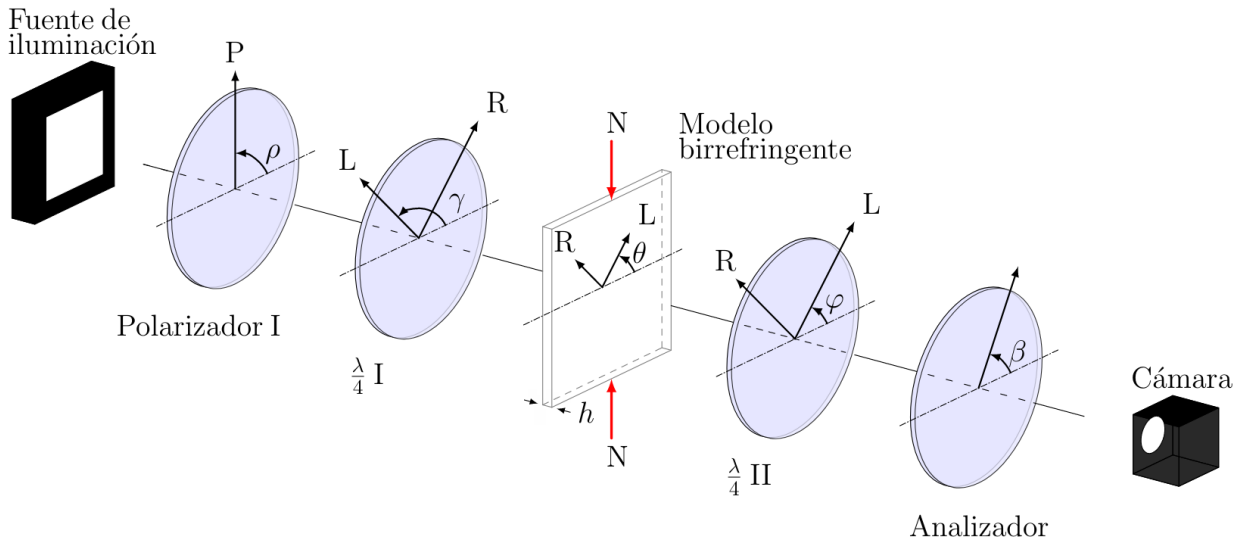
In Figure 1, the parameters refer to the angles of the relative orientations of the linear polarizers and quarter-wave retarders, respectively. This polariscope is said to be circular because the light emerging from the illumination source, before hitting the model, is circularly polarized by effects of the linear polarizer I and the quarter-wave retarder I.

In experimental studies of photoelasticity, the set of images to calculate a stress field can be obtained by: (1.) varying the optical configurations of the polariscope used; (2.) varying the load applied to the model; or (3.) varying the wavelength of the polariscope illumination source. In computational studies, steps (1.), (2.) and (3.) can be simulated, as shown in this paper.

From the set of fringe pattern images, a wrapped phase delay map is obtained, which requires additional processing to achieve a continuous phase, or unwrapped phase, delay map. Among the approaches to compute the wrapped phase map, two stand out: phase-variant fringe shift and load-variant fringe shift.

The first approach is called Phase Shifting - PS-, and generally refers to a family of methods that process collections of images with fringe shifts produced by small changes in the optical configurations of the polariscope: rotations of its optical elements. One PS method that has been shown to be very effective is the method of Wang and Patterson [15], which uses

Figure 1. Detail of a circular polariscope.



Source: own.

six optical configurations of a circular polariscope to produce an equal number of images with fringe patterns. Several studies have documented the effectiveness of Wang and Patterson's method [15] in stress field recovery. However, its implementation is not without problems, because in four of the six images required by the method, there is interaction between the isoclinic and isochromatic parameters. Additionally, the implementation of this method produces areas of inconsistencies and ambiguities, which must be resolved before the wrapped phase map is calculated. In practical implementations, it has been documented that the polariscope configurations required by this method are a source of problems in photoelasticity studies, since even small misalignments produce errors in the subsequent reconstruction of the stress field.

In this paper, the second approach to calculate wrapped phase maps is considered: load stepping. Hereafter, the acronym LS will be used to refer to this method, since in English it is called *Load Stepping*. This method differs from PS in that the collection of images with fringe shifts is achieved by inducing small variations to the reference load P applied to the model. Equations (9) to (14) are the analytical expressions for calculating the six images required by the LS method. A feature of this method is that all the required images are obtained with only two polariscope configurations. In experimental problems, this feature allows to reduce the amount of processing required to obtain the wrapped phase delay map.

$$I1 = \frac{1}{n} \int_{\lambda=\lambda_0}^{\lambda=\lambda_n} \frac{I_a(\lambda)}{2} [1 + \cos \cos(\delta)] * S_{RGB}(\lambda) d\lambda \quad (9)$$

$$I2 = \frac{1}{n} \int_{\lambda=\lambda_0}^{\lambda=\lambda_n} \frac{I_a(\lambda)}{2} [1 - \cos \cos(\delta)] * S_{RGB}(\lambda) d\lambda \quad (10)$$

$$I3 = \frac{1}{n} \int_{\lambda=\lambda_0}^{\lambda=\lambda_n} \frac{I_a(\lambda)}{2} [1 + \cos \cos(\delta + \Delta\delta)] * S_{RGB}(\lambda) d\lambda \quad (11)$$

$$I4 = \frac{1}{n} \int_{\lambda=\lambda_0}^{\lambda=\lambda_n} \frac{I_a(\lambda)}{2} [1 - \cos \cos(\delta + \Delta\delta)] * S_{RGB}(\lambda) d\lambda \quad (12)$$

$$I5 = \frac{1}{n} \int_{\lambda=\lambda_0}^{\lambda=\lambda_n} \frac{I_a(\lambda)}{2} [1 + \cos \cos(\delta - \Delta\delta)] * S_{RGB}(\lambda) d\lambda \quad (13)$$

$$I6 = \frac{1}{n} \int_{\lambda=\lambda_0}^{\lambda=\lambda_n} \frac{I_a(\lambda)}{2} [1 - \cos \cos(\delta - \Delta\delta)] * S_{RGB}(\lambda) d\lambda \quad (14)$$

In equations (9) to (14), $+\Delta\delta$ refers to a phase delay, which results by producing a variation in the charge ΔP . Table 1 shows the polariscope configurations required to obtain the images I1, ... I6.

Table 1. Intensity equations and rotations of the optical elements in a circular polariscope, for the LS method of Ekman and Nurse [13]. These rotation angles are shown graphically in Figure 1.

Equation	ρ	γ	φ	β
I1	90	45	-45	90
I2	90	45	-45	0
I3	90	45	-45	90
I4	90	45	-45	0
I5	90	45	-45	90
I6	90	45	-45	0

Source: own.

From the intensity images calculated with Equations (9) to (14), the LS method provides a strategy to calculate a wrapped phase delay map. This strategy is achieved by applying Equations (15), (16), (17) and (18).

$$ID1 = \frac{I1 - I2}{2} \quad (15)$$

$$ID2 = \frac{I3 - I4 + I5 - I6}{4} \quad (16)$$

$$ID3 = \frac{I5 - I6 - I3 + I4}{4} \quad (17)$$

$$\delta = \arg \left(ID2 * \tan \tan \left(\cos^{-1} \left(\frac{ID2}{ID1} \right) \right) + i ID3 \right) \quad (18)$$

In this work, discontinuous phase maps are unwrapped using the method of Ghiglia and Romero [16].

2.2. Thermoelastic stress analysis

Thermoelastic Stress Analysis (TSA) is a non-invasive technique for quantifying temperature changes in materials subjected to cyclic loading. It has been documented that in orthotropic and homogeneous materials, there is a linear relationship between

temperature changes and the difference of the sum of the rectangular stresses. This relationship is described by Equation (19).

$$\Delta T = -K * \Delta(\sigma_{xx} + \sigma_{yy}) \quad (19)$$

$$K = \frac{\alpha T}{\rho C_p} \quad (20)$$

In Equation (19), the term K is called the thermoelastic constant of the material, which in turn is expressed by Equation (20), where ρ is the density of the material, C_p is the specific heat and α is the linear coefficient of thermal expansion. The result of applying the thermoelastic effect computationally is a digital image that is in fact a thermogram: an image with a temperature field that, in practice, can be acquired with a thermographic camera.

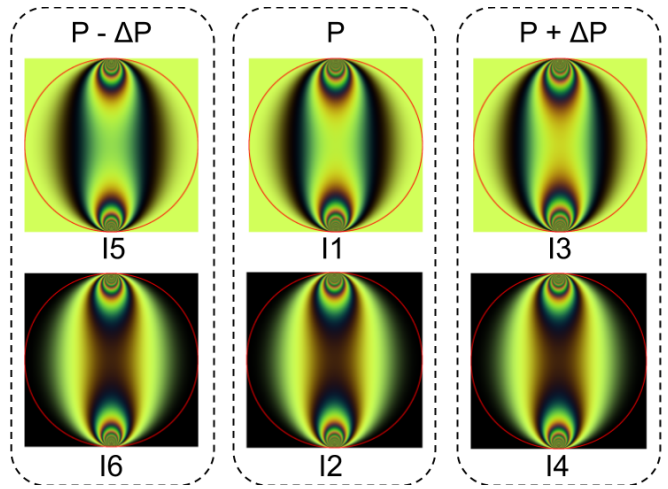
Experimentally, a TSA study requires that the load variations applied to the sample under inspection be made at a sufficiently fast rate, so that the temperature increases are not dissipated in the sample geometry; i.e., that the experiments be made under an adiabatic condition.

In this paper, it is assumed that the computational experiments comply with the adiabatic condition, so that the thermal field of the considered model can be calculated. But, in addition, it is assumed that the load variations conform to those required by an LS experiment. Under these assumptions, the thermal and stress field of the model could be calculated with a single integration experiment.

3. Materials and Methods

The experimentation presented in this paper is based on the generation of a set of color images $I_1 \dots I_6$, as used by the LS method of Ekman and Nurse [13]. An example set of images is shown in Figure 2.

Figure 2. Example of images with fringe shifts, as used by the LS algorithm.

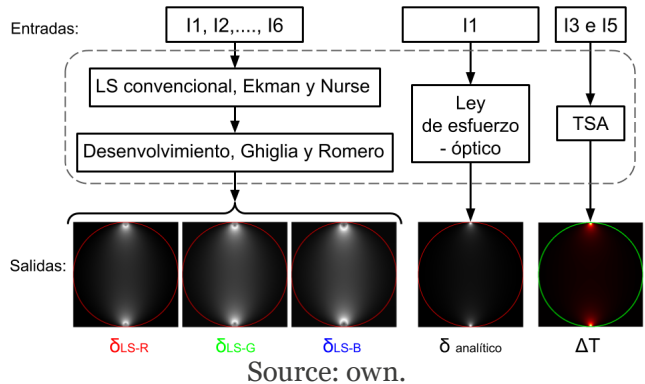


Source: own.

The six images are divided into three pairs, for which the charge applied to the sample is the same. Each pair includes one image in brightfield polariscope configuration and one in darkfield configuration.

Given a set of computational color images as in Figure 2, the method of Ekman and Nurse [13] is applied on the three color components R, G and B, resulting in three wrapped phase maps. After applying the method of Ghiglia and Romero [16], three unwrapped phase maps are arrived at, as shown in Figure 3.

Figure 3. Phase delay maps and temperature map, for a reference load P , from the set of images for an experiment with the Ekman and Nurse method [13].



Source: own.

The theoretical basis for integrating LS, a photoelasticity technique, with thermoelasticity lies in the following fact: the charge difference between the steps $(P + \Delta P)$ and $(P - \Delta P)$, can be used to produce a temperature signal using the thermoelastic effect of Equation (19).

Figure 3 shows that from I_1 an analytical map of phase delays can be calculated. Likewise, with images I_3 and I_5 a map of temperature increments ΔT can be obtained, using the thermoelastic effect. In summary, Figure 3 indicates that theoretically, the set of computational images required in an LS experiment can also be used to obtain a TSA signal. The techniques that apply to each subset of the images $I_1 - I_6$ are enclosed by the dashed line.

In a practical experiment, the integration would demand that the change between the loading steps ($P + \Delta P$) and ($P - \Delta P$) be made fast enough to guarantee the adiabatic condition, and simultaneously allow the stress field for the reference load P to be reconstructed.

3.1. Computational integration experiment.

To generate the images required by the LS method, three loads are required: a reference load P , and two load steps $P + \Delta P$ and $P - \Delta P$. In this paper, a general experiment is considered, where the set of images is generated for fifty reference load values P . For each of these P values, (a) the stress field using the LS method and (b) the temperature field using the thermoelastic effect are calculated. The fifty P values are linearly distributed between 1 and 2500N. Regarding how the loading steps occur, there are two variants of this general experiment.

In the first variant, the increment ΔP is equal to 10% of the reference value P . This means that for each reference load the steps $P + 0.1 \cdot P$ and $P - 0.1 \cdot P$ are calculated, and then the stress and temperature field is calculated. This variant aims at stress field recovery using the LS method. The six images are processed to obtain three unwrapped phase maps, as shown graphically in Figure 3; one for each color channel. Each map is compared with the analytical phase retardation map obtained for P . In parallel, the average and maximum temperature values achieved in the thermoelasticity experiment are recorded.

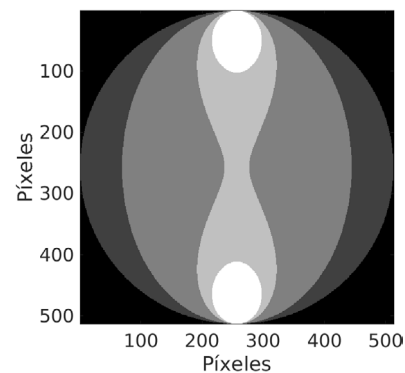
In the second variant of the general experiment, the same percentage of 10% is used to produce the step $P + \Delta P$. However, the $P - \Delta P$ step is replaced by a charge equal to zero Newtons. This experimental variant aims more towards the generation of the TSA signal. In practice, such an experiment can be achieved by applying impact loads, as shown in the work of Vergara and colleagues [17].

Since the TSA signal is obtained from an applied load difference, the change by zero Newtons instead of $P - \Delta P$, induces a larger stress difference when applying the thermoelastic effect.

3.2. Segmentation of the high stress concentration zone

The unwrapped phase retardation and temperature maps are analyzed only in the zone of the disk that experiences a high stress concentration. To define this zone, an additional simulation is carried out, where a PMMA disk is subjected to diametral compression with a load of 3500 N. Then, the zones within the disk where the difference of the principal stresses is equal or greater than 56 MPa, which corresponds to 80% of the yield stress reported for PMMA, are detected. These zones of high stress concentration are shown in white in the image of Figure 4. Since there are two zones where the stress information is exactly the same, it was decided to work only with the upper zone.

Figure 4. In white, the areas with the highest stress concentration for a PMMA disc under diametral compression.



Source: own.

In digital photoelasticity studies, it has been documented that areas where the fringe concentration is very high, the stress concentration is also very high. A very high closeness between fringes makes them indistinguishable, and the region looks uniform, even though it experiences high stresses. It has also been documented that in these zones where the fringe patterns are indistinguishable, the algorithms for calculating the stress field have performance problems.

3.3. Scope of the Integration Strategy

The integrated computational approach provides two outputs for each reference load P . The first is a set

of three phase delay maps, one for each color channel. The second output is a temperature map.

To analyze the effect of the reference load P and of the loading steps on the ability to reconstruct the stress field, the differences between the phase delay maps obtained via LS and the analytical maps are analyzed. For this purpose, *Mean Square Error* (MSE) and structural similarity values are calculated between each of these three maps and the respective analytical map. The structural similarity values are calculated using the *Structural Similarity Index* (SSIM) proposed by Wang and colleagues [18].

Separately, for each load value P , the average and maximum temperature values in the region under consideration are measured. When plotting these temperature values, they are plotted against the applied load difference, and not against the reference load P .

4. Results

4.1. Analysis of the digital photoelasticity experiment

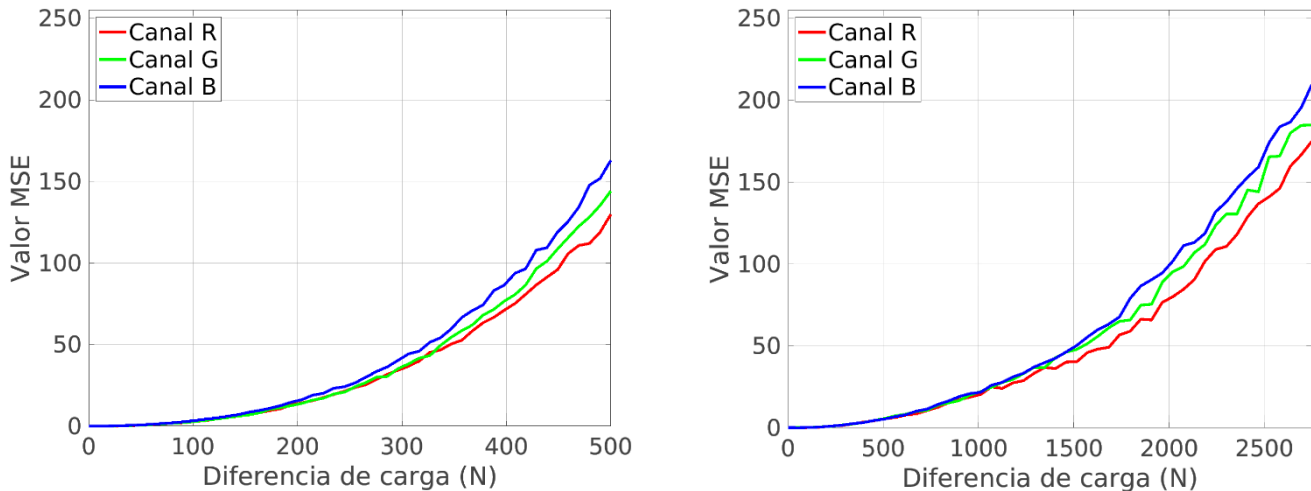
Figure 5 shows the mean square error values that would be achieved in the two variants of the overall

experiment. A first result is that variant 2 causes larger differences between the analytical and LS unwrapped phase delay maps. The importance of this result lies in the fact that the second variant of the general experiment produces higher temperatures, so they would be detected with less difficulty with the considered thermal imager. However, the higher temperature values would be obtained at the expense of a higher error in the stress field reconstruction.

A second result is that the error in the unwrapped phase maps varies with color channel. This can be explained as a consequence of the stress-optical law, since the modulation of fringe patterns is an inverse function of wavelength. According to this law, higher fringe densities and hence higher modulation are expected for the blue channel. The plots in Figure 6 show the measured structural similarity values between the analytical stress maps and those obtained by LS.

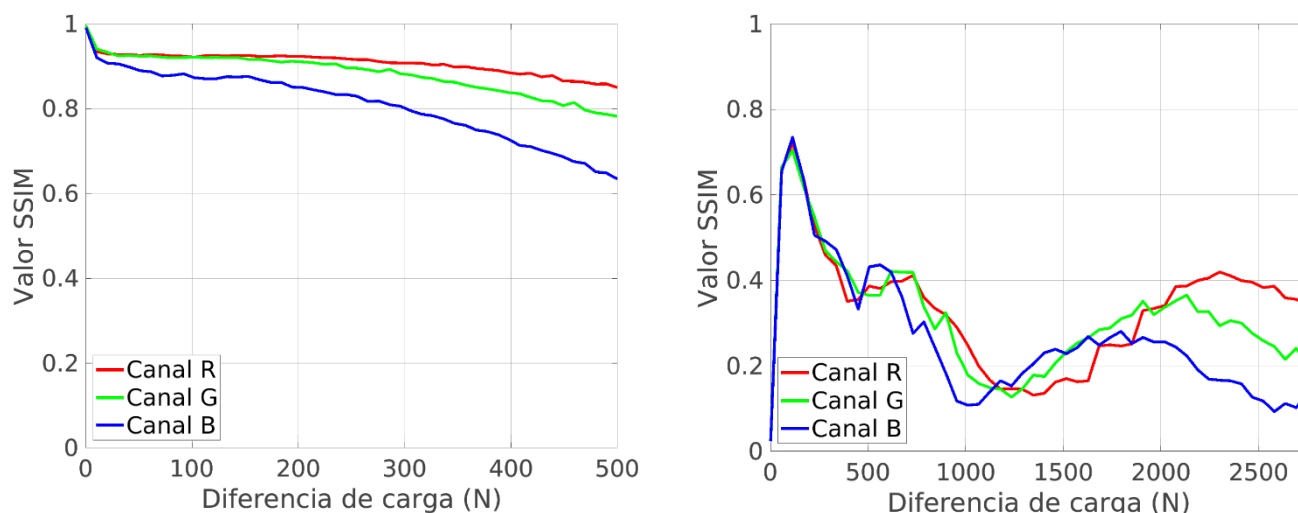
When comparing the SSIM values achieved with variants 1 and 2, it is observed that the increase in load difference produces a considerable decrease in the structural similarity index. This result indicates that higher applied load differences affect the reconstruction of the stress field using LS. To explain the results in the

Figure 5. The left and right graphs show, in this order, the mean squared error -MSE- values for load variations in variants 1 and 2 of the general experiment.



Source: own.

Figure 6. From left to right, structural similarity index -SSIM- values for load variations in variants 1 and 2 of the general experiment.

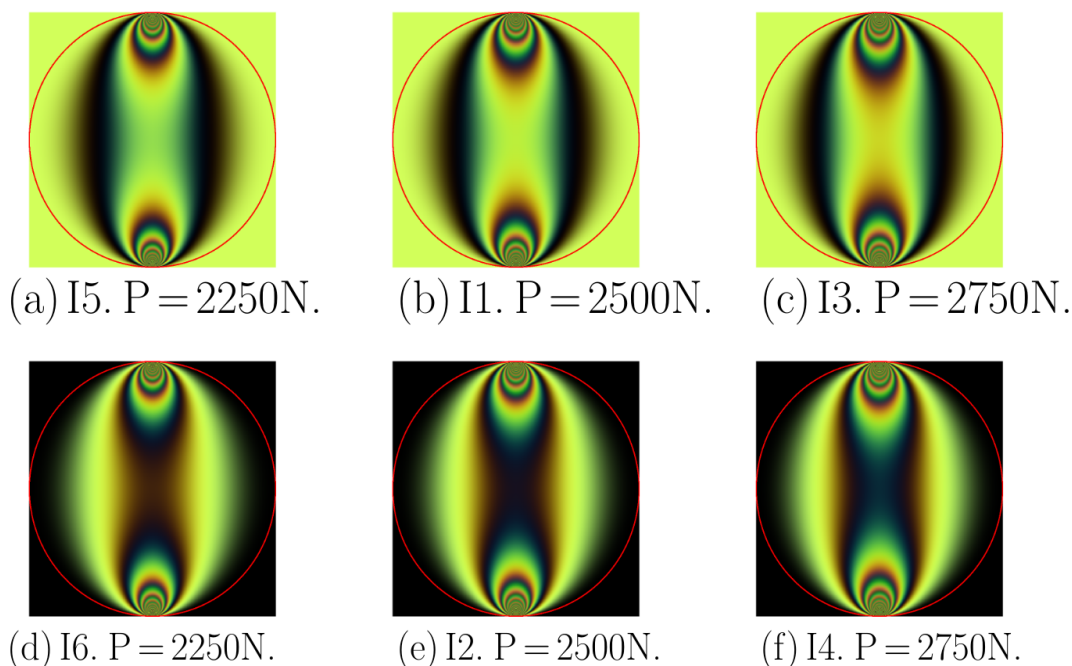


Source: own.

plots in Figure 6, the results are analyzed for the case where the reference load $P = 2500\text{N}$, in the two variants of the general integration experiment.

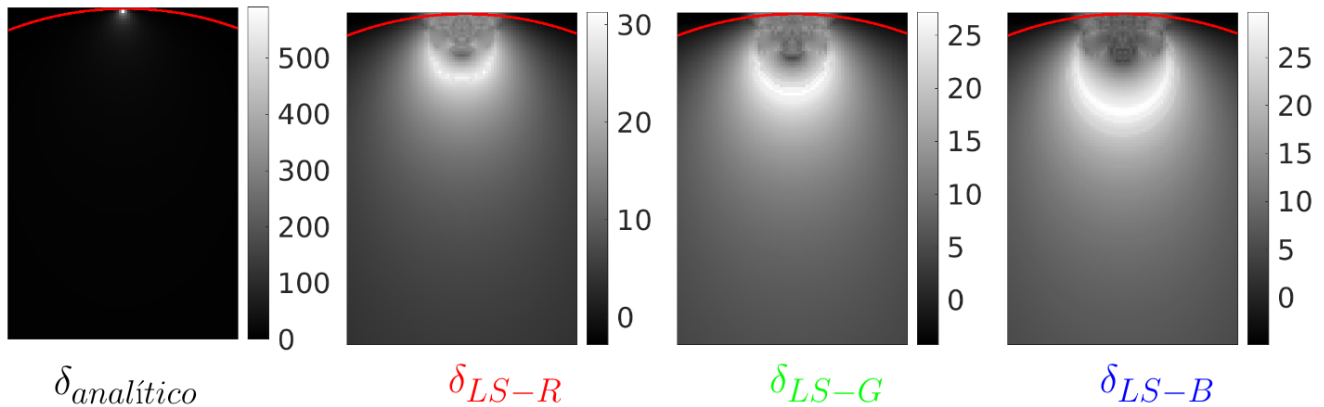
Initially, Figure 7 shows the intensity images for variant 1, which is when the load steps are equal to 10% of the reference load P . By applying the LS method to these color images, the phase delay maps shown in Figure 8 are obtained.

Figure 7. Color intensity images for variant 1 of the general experiment.



Source: own.

Figure 8. Representation of analytical phase delay map and unwrapped phase delay maps for each color channel for variant 1 of the overall experiment.

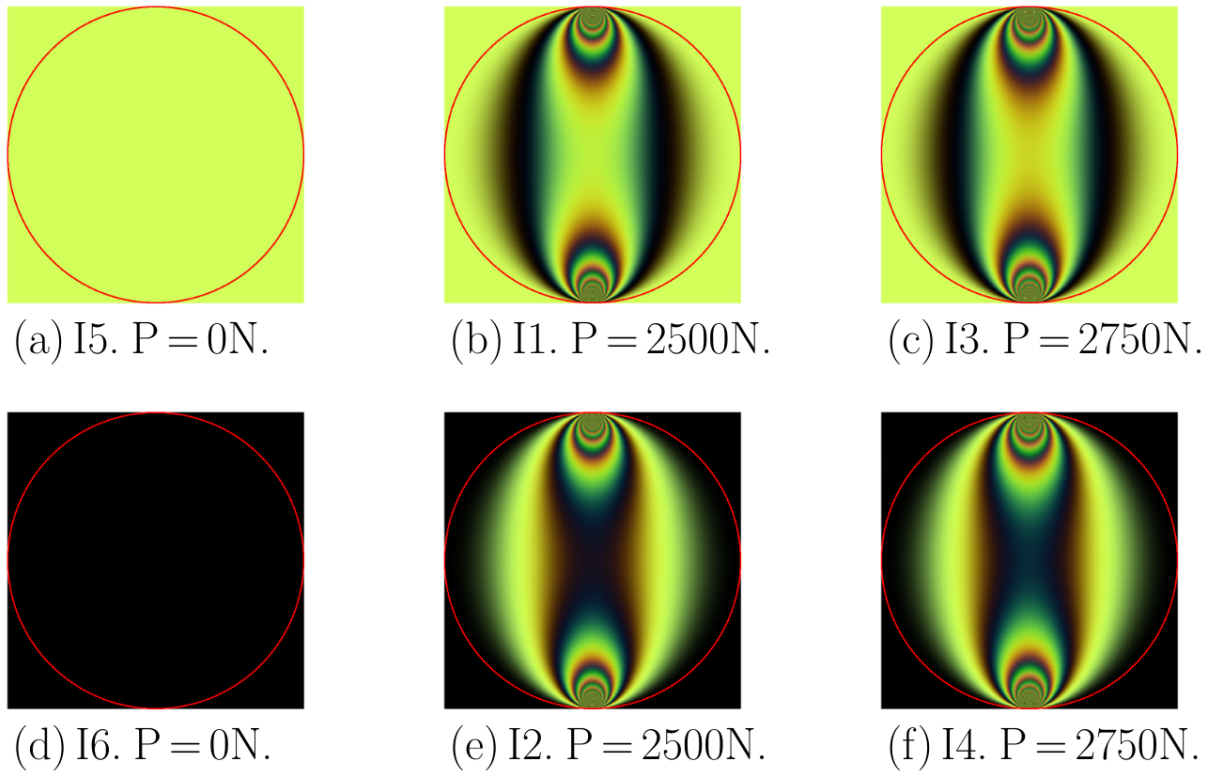


Source: own.

Additionally, the unwrapped phase delay maps in Figure 8 indicate that the maximum fringe orders achieved per color channel are far from those obtained with the analytical delay map.

The results for variant 2 are shown in Figures 9 and 10. The intensity images for this second case are shown in Figure 9. There, one particularity is observed and that is that the images for the P - ΔP loading step do not have fringe patterns.

Figure 9. Color intensity images for variant 2 of the general experiment.



Source: own.

The unwrapped phase delay maps obtained with the images in Figure 9 are shown in Figure 10. The most important information in these maps is the appearance of negative fringe orders. Additionally, the fringe orders in these maps are lower than those obtained with variant 1. This result reaffirms the idea that, increasing the stress difference to achieve higher temperature values in the integration experiment would negatively affect the ability to reconstruct the stress field of the birefringent model under loading.

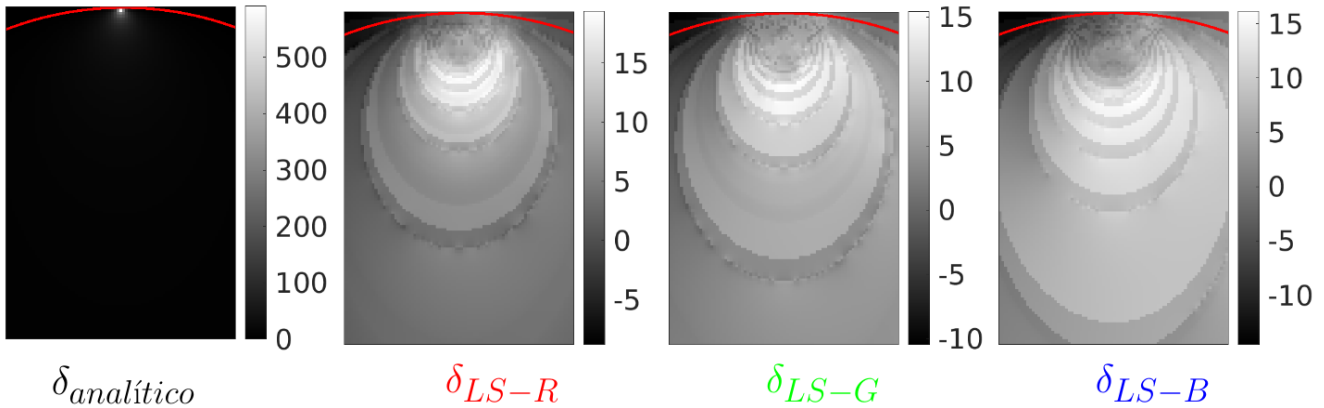
4.2. Analysis of the thermoelasticity experiment

Figure 11 shows the average and maximum temperature values that would be obtained for the two variants of the general experiment.

The magenta horizontal line in both graphs is the thermal sensitivity value of a FLIR A65 camera, which is used as a reference. This parameter is called *Noise Equivalent Temperature Difference*, or NETD, and refers to the minimum difference in temperature values that the camera can detect. The importance of NETD in this graph is as follows: temperature values below the NETD value represent noise, and the camera will not register them as significant temperature values in a thermal image. The right graph indicates that increasing the load difference applied to the model has a significant impact on the maximum values that would be achieved in the TSA experiment.

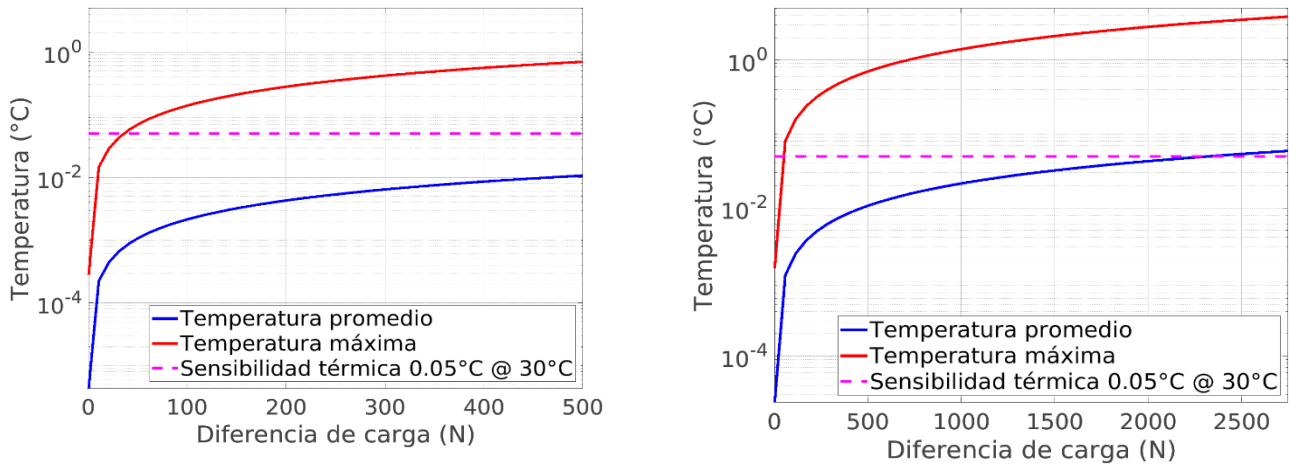
Variant 1 of the general experiment would produce average temperature values that would be below the

Figure 10. Representation of analytical phase delay map and unwrapped phase delay maps for each color channel for variant 2 of the general experiment.



Source: own.

Figure 11. From left to right, mean and maximum temperature values, for load variations according to experiments 1 and 2, respectively.



Source: own.

sensitivity threshold of the chamber. This, even in the disk area where very high stress and temperature levels are expected due to its proximity to the load application point. With variant 2, average temperatures above the sensitivity of the chamber would be reached for applied load differences close to 400N. Maximum temperatures would be above this threshold.

These results indicate that, for thermographic analysis, both experiments will produce temperature values that would be recorded by the thermographic camera under consideration. However, there would be fewer difficulties with variant 2, because the temperatures achieved would be higher.

5. Conclusions

This paper presented the results of a computational study, which aimed at the integration of digital photoelasticity and thermoelastic stress analysis. The integration consisted of implementing the method of fringe displacements by load variation, under the assumption that the load jumps are applied with sufficient velocity to generate an adiabatic condition.

As a general conclusion of the computational experiments, it is theoretically possible to obtain the stress and temperature fields of a birefringent model under load from a single experiment where variable load is applied.

However, this integration experiment would have the following limitations: if the loading steps are small, as recommended in LS experiments, then the temperature values obtained by TSA would also be very small, which would make the analyses difficult from the thermoelastic point of view. It is possible to increase the applied load differences, to produce higher temperature values. However, if the load displacements are too large then they will affect the stress field reconstruction that would be achieved with the LS technique.

As future work, it will be necessary to develop a methodology to determine the optimal loading steps to achieve stress field reconstruction while achieving the highest possible temperature rise.

Acknowledgments

The authors express their gratitude to the “Jóvenes Investigadores” program of the Instituto Tecnológico Metropolitano, and to the “Extendiendo Fronteras” program of the Medellín Agency for Higher Education - Sapiencia.

References

- [1] K. Ramesh y S. Sasikumar, “Digital photoelasticity: Recent developments and diverse applications”, *Optics and Lasers in Engineering*, vol. 135, pp. 106186, 2020. <https://doi.org/10.1016/j.optlaseng.2020.106186>
- [2] A. Ajovalasit, G. Petrucci y M. Scafidi, “Review of RGB photoelasticity”, *Optics and Lasers in Engineering*, vol. 68, pp. 58-73, 2015. <https://doi.org/10.1016/j.optlaseng.2014.12.008>
- [3] G. Pitarresi, R. Cappello y G. Catalanotti, “Quantitative thermoelastic stress analysis by means of low-cost setups”, *Optics and Lasers in Engineering*, vol. 134, pp. 106158, 2020. <https://doi.org/10.1016/j.optlaseng.2020.106158>
- [4] S. Barone y E. A. Patterson, “Full-field separation of principal stresses by combined thermo- and photoelasticity”, *Experimental Mechanics*, vol. 36, no. 4, pp. 318–324, 1996. <https://doi.org/10.1007/BF02328573>
- [5] B. V. Farahani, P. J. Tavares, P. M. Moreira, y J. Belinha, “Stress intensity factor calculation through thermoelastic stress analysis, finite element and RPIM meshless method”, *Engineering Fracture Mechanics*, vol. 183, pp. 66-78, 2017. <https://doi.org/10.1016/j.engfracmech.2017.04.027>
- [6] R. J. Greene, A. B. Clarke, S. Turner, y E. A. Patterson, “Some applications of combined thermoelastic-photoelastic stress analysis”, *The Journal of Strain Analysis for Engineering Design*, vol. 42, no 3, pp. 173-182, 2007. <https://doi.org/10.1243/03093247JSA134>
- [7] T. SAKAI, Y. IIHARA y S. YONEYAMA, “Analysis of Fiber-Matrix Interfacial Stresses Using Experimental-numerical Hybrid Technique”,

- Journal of the Japanese Society for Experimental Mechanics, vol. 15, no. 3, pp. 169-174, 2015. <https://doi.org/10.11395/jjsem.15.169>
- [8] T. Sakagami, S. Kubo, Y. Fujinami, y Y. Kojima, “Experimental stress separation technique using thermoelasticity and photoelasticity and its application to fracture mechanics”, JSME International Journal Series A Solid Mechanics and Material Engineering, vol. 47, no. 3, pp. 298-304, 2004. <https://doi.org/10.1299/jsmea.47.298>
- [9] M. Solaguren-Beascoa, J. M. Alegre, P. M. Bravo y I. I. Cuesta, “Stress-separation techniques in photoelasticity: a review”, The Journal of Strain Analysis for Engineering Design, vol. 45, no. 1, pp. 1-17, 2010. <https://doi.org/10.1243/03093247JSA583>
- [10] D. Rezini, T. Baki, y Y. Rahmani, “A new concept of plane stress analysis of notched flat bar in axial tension”, Archive of Applied Mechanics, vol. 86, no. 8, pp. 1483-1494, 2016. <https://doi.org/10.1007/s00419-016-1130-z>
- [11] S. Yoneyama, S. Arikawa y Y. Kobayashi, “Linear and nonlinear algorithms for stress separation in photoelasticity”, Experimental mechanics, vol 52, no. 5, pp. 529-538, 2012. <https://doi.org/10.1007/s11340-011-9512-1>
- [12] S. Barone y E. A. Patterson, “Development of simultaneous thermo- and photo-elasticity for principal stress analyses,” Strain, vol. 35, no. 2, pp. 57–65, 1999, <https://doi.org/10.1111/j.1475-1305.1999.tb01127.x>
- [13] M. J. Ekman y A. D. Nurse, “Completely automated determination of two-dimensional photoelastic parameters using load stepping”, Optical Engineering, vol. 37, no. 6, pp. 1845-1851, 1998. <https://doi.org/10.1117/1.601694>
- [14] J. C. Briñez, A. Restrepo-Martínez, y J. W. Branch, “Computational hybrid phase shifting technique applied to digital photoelasticity”, Optik, vol. 157, pp. 287-297, 2018. <https://doi.org/10.1016/j.jleo.2017.11.060>
- [15] E. A. Patterson, “Digital photoelasticity: Principles, practice and potential,” Strain, vol. 38, no. 1, pp. 27–39, 2002, <https://doi.org/10.1046/j.0039-2103.2002.00004.x>
- [16] D. C. Ghiglia y L. A. Romero, “Robust two-dimensional weighted and unweighted phase unwrapping that uses fast transforms and iterative methods”, Journal of the Optical Society of America A, vol. 11, no. 1, p. 107, 1994. <https://doi.org/10.1364/JOSAA.11.000107>
- [17] R. Vergara-Puello, H. A. Fandiño-Toro y A. Restrepo-Martínez, “Stresses analysis through digital photoelasticity and infrared thermography in an epoxy sample affected by cyclic loads: a cost-effective proposal”, In Optics and Photonics for Information Processing XIV, pp. 115090B, 2020. <https://doi.org/10.1117/12.2568780>
- [18] Z. Wang, A. C. Bovik, H.R. Sheikh, y E. P. Simoncelli, “Image quality assessment: from error visibility to structural similarity”, IEEE transactions on image processing, vol. 13, no. 4, pp. 600-612, 2004, <https://doi.org/10.1109/TIP.2003.819861>
- [19] S. T. Piracoca-Peralta, E. Rivas-Trujillo, H. Montaña-Quintero, “Generador axial para un generador eólico de baja potencia, selección, diseño y simulación en COMSOL multiphysic”, Vis. Electron., vol. 15, no. 1, 2021. <https://doi.org/10.14483/22484728.17985>